

**Microwave analog of Stern-Gerlach effects using nonuniform chiral metamaterials**Satoshi Tomita,<sup>1,\*</sup> Kei Sawada,<sup>2</sup> Shotaro Nagai,<sup>3</sup> Atsushi Sanada,<sup>4</sup> Nobuyuki Hisamoto,<sup>5</sup> and Tetsuya Ueda<sup>5</sup><sup>1</sup>*Graduate School of Materials Science, Nara Institute of Science and Technology, 8916-5 Takayama, Ikoma, Nara 630-0192, Japan*<sup>2</sup>*RIKEN SPring-8 Center, 1-1-1 Kouto, Sayo, Hyogo 679-5148, Japan*<sup>3</sup>*Graduate School of Science and Engineering, Yamaguchi University, 2-16-1 Tokiwadai, Ube, Yamaguchi 755-8611, Japan*<sup>4</sup>*Graduate School of Engineering Science, Osaka University, 1-3 Machikaneyama, Toyonaka, Osaka 560-8531, Japan*<sup>5</sup>*Department of Electronics, Kyoto Institute of Technology, Matsugasaki, Sakyo, Kyoto 606-8585, Japan*

(Received 23 February 2017; revised manuscript received 15 September 2017; published 13 October 2017)

This study observes microwave beam splitting dependent on circular polarizations through nonuniform chiral metamaterials. Nonuniform chiral metamaterials with a gradation in refractive index are constructed using chiral meta-atoms that exhibit optical activities at microwave frequencies. Microwave scattering far-field patterns by the nonuniform chiral metamaterials demonstrate a deflection of microwaves, which transmit in a direction perpendicular to the refractive index gradient. Furthermore, circularly polarized microwaves with opposite “spins of light” go their separate ways in the nonuniform chiral metamaterials. This phenomenon is an optical analog of the Stern-Gerlach effects for electrons.

DOI: [10.1103/PhysRevB.96.165425](https://doi.org/10.1103/PhysRevB.96.165425)**I. INTRODUCTION**

The Stern-Gerlach (SG) experiment [1] is a milestone in the history of quantum theory [2]. In the SG effects, particles with opposite spins with nonzero magnetic moments will go their separate ways in a nonuniform magnetic field. Historically the SG effects demonstrated existence of an electronic spin degree of freedom. The spin magnetic moment is coupled to the magnetic field that breaks the time-reversal symmetry. Once the existence of the electron spin was proved, utilization of the spin-orbit interaction by breaking the space-inversion symmetry was another way to obtain spin-dependent phenomena.

In an analogy between electrons and photons, optical analogs of the SG effects are of great interest. A similar effect for unpolarized light was experimentally observed as the electromagnetically-induced transparency (EIT) enhanced deflection [3]. The spatial motion of light in the EIT atomic ensemble has been explained by a semiclassical theory based on the spatial dependence of the refractive index [4] and by a fully quantum approach [5]. The EIT-enhanced deflection of nonpolarized light cannot be, however, explained as an optical analog of the SG effects because only one component of “the spin” is available [6]. An atomic beam SG analog is only applicable for light in polarized materials. The decomposition of a light ray into two rays dependent on the polarization is classically formalized by assigning two different refractive indices of the materials for different polarization.

Chiral material with broken space-inversion symmetry is characterized by two indices of refraction: one for left-handed circularly polarized (LHCP) and one for right-handed circularly polarized (RHCP) light. Linearly polarized light is regarded as a coherent superposition of LHCP and RHCP light. Fresnel’s theory of optical rotation indicates that a difference in the refractive indices causes the waves to acquire phase difference as they propagate through chiral medium, that is to say, optical activity [7–9]. Furthermore, when linearly

polarized light is incident from an achiral medium to a chiral medium, the light will split into two beams: one LHCP and the other RHCP [10]. Such a split of light into two beams was experimentally demonstrated using light reflection and refraction with an oblique incidence into a uniform chiral liquid containing natural chiral molecules [11]. While refraction into uniform chiral media with an oblique incidence corresponds to transmission into nonuniform chiral media with a normal incidence, direct observation of the SG effects for light is lacking because it is a challenge to prepare nonuniform chiral media using natural chiral molecules.

This paper reports a microwave analog of the SG experiment using nonuniform chiral metamaterials. Metamaterials and metasurfaces enable us to realize unusual optical properties with well-designed subwavelength-sized structures [12–17]. Previously we have studied optical activities of a Cu chiral structure—chiral meta-atom—at microwave frequencies [18,19]. Here, the chiral meta-atoms are used to construct nonuniform chiral metamaterials with refractive index gradient. An atomic beam, electron spin, gauge field, and the nonuniform magnetic field in the original SG experiment correspond, respectively, to a microwave, circular polarization, electromagnetic induction by chiral materials, and the nonuniform distribution of the chiral meta-atoms in our experiment. Microwave scattering far-field patterns through nonuniform chiral metamaterials with normal incidence are measured as a function of frequency and deflection angle in free space. Transmitted microwaves are deflected by the nonuniform chiral metamaterials. Moreover, LHCP and RHCP microwaves go their separate ways in the nonuniform chiral metamaterials. The splitting is traced back to “magnetic field” for microwaves. Since materials are regarded as fields by electromagnetic waves, the present study is one further step for synthetic gauge fields for light [20–25] using metamaterials.

This paper is organized in six sections. Section II describes the theoretical background of the SG effects for light. Section III details the experimental procedures including preparations of uniform/nonuniform chiral metamaterials and measurements of microwave scattering far-field patterns in the free space. Section IV illustrates the experimental results of

\*tomita@ms.naist.jp

the microwave transmission amplitude patterns through uniform/nonuniform chiral metamaterials received by a rectangle horn antenna or LHCP/RHCP antenna. Section V presents discussion on microwave amplitude difference patterns and the SG effects for microwaves using nonuniform chiral metamaterials, and conclusions are given in Sec. VI.

## II. THEORETICAL BACKGROUND

In this section, we present theoretical background of the SG effects for light. Maxwell equations for plane waves are written as

$$\vec{k} \times \vec{E}(\vec{r}) = \omega \vec{B}(\vec{r}), \quad (1)$$

$$\vec{k} \times \vec{H}(\vec{r}) = -\omega \vec{D}(\vec{r}), \quad (2)$$

where  $\vec{k}$ ,  $\vec{E}$ , and  $\vec{H}$  are the wave vector, the electric field, and the magnetic field, respectively. The electric flux density  $\vec{D}$  and the magnetic flux density  $\vec{B}$  in isotropic chiral media are given by constitutive equations,

$$\vec{D} = \varepsilon_0 \varepsilon \vec{E} - i \frac{\xi}{c} \vec{H}, \quad (3)$$

$$\vec{B} = \mu_0 \mu \vec{H} + i \frac{\xi}{c} \vec{E}, \quad (4)$$

where  $\varepsilon$  and  $\mu$  are the electric permittivity and magnetic permeability of the media, respectively.  $\varepsilon_0$  and  $\mu_0$  are, respectively, the electric permittivity and magnetic permeability of vacuum. The chiral parameter  $\xi$  gives rise to electromagnetic induction in the media, resulting in optical activities. The speed of light in vacuum is represented by  $c = \frac{1}{\sqrt{\varepsilon_0 \mu_0}}$ .

For simplicity, we assume electromagnetic waves propagating direction to be parallel to the  $z$  direction;  $\vec{k} = (0, 0, k)$ . The eigenmodes are written as  $\vec{E} = \frac{1}{\sqrt{2}}(E, \pm iE, 0)$ , where  $+$  and  $-$  represent left- and right-handed circular polarizations, respectively. These states correspond to ‘‘spin states’’ of photons. Given Eqs. (1)–(4), the dispersion relation is obtained to be

$$\frac{\omega^2}{c^2} \varepsilon \mu \mp 2k\xi \frac{\omega}{c} - k^2 = 0. \quad (5)$$

The refractive index  $n = c|\vec{k}|/\omega$  is calculated to be

$$n_L = n_0 - \xi \hat{k}, \quad (6)$$

$$n_R = n_0 + \xi \hat{k}, \quad (7)$$

where  $n_0 = \sqrt{\varepsilon} \sqrt{\mu}$ , the higher order terms of  $\xi$  are neglected, the subscripts L and R correspond to left- and right-handed circular polarizations, and  $\hat{k} = k/|k| = \text{sgn}(k)$ . As shown in Fig. 1(a), the dispersion curve in the chiral media splits for each polarization state;  $\omega_L(k) \neq \omega_R(k)$ . Given the time-reversal symmetry, the dispersion satisfies the relation,

$$\omega_L(k) = \omega_R(-k), \quad \omega_R(k) = \omega_L(-k). \quad (8)$$

This implies that a mode with  $(\omega, k, R)$  has always its counterpart with  $(\omega, -k, L)$  of the different polarization propagating to the opposite direction. Such a dispersion is analogous to that in electronic systems with spin-orbit interactions.

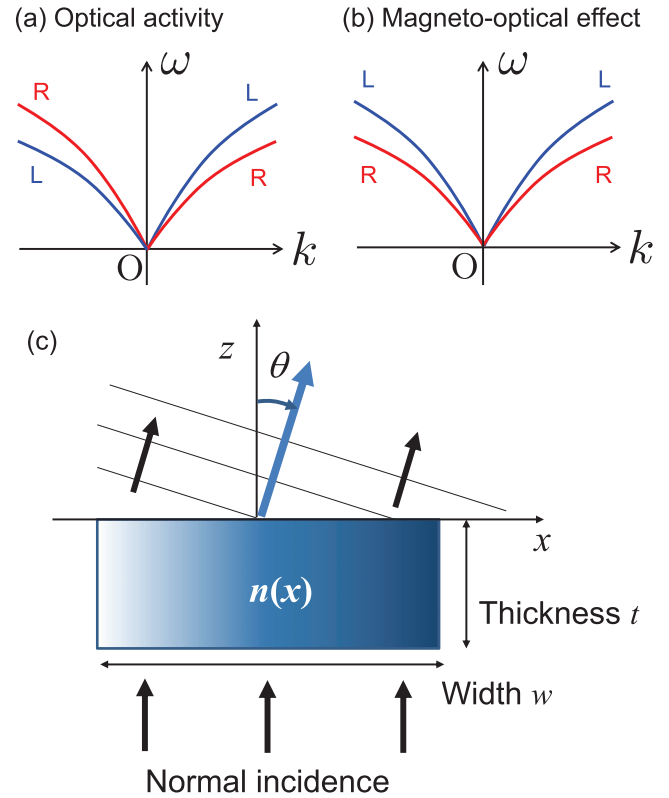


FIG. 1. Dispersion relations in (a) chiral and (b) magneto-optical media. (c) A normal incidence to a medium with the refractive index gradient  $n(x)$  in a direction perpendicular to the incident direction.

It is useful to compare this case with a distinct case in which the time-reversal symmetry is broken but the space-inversion symmetry is unbroken, i.e., magnetic systems. In magnetic systems, when electromagnetic waves propagate parallel to the magnetization and/or the external magnetic field, the dispersion relation splits with circular polarizations as shown in Fig. 1(b). These are so-called magneto-optical effects. From the space-inversion symmetry, the dispersion satisfies the relation

$$\omega_L(k) = \omega_L(-k), \quad \omega_R(k) = \omega_R(-k). \quad (9)$$

It is analogous to electronic dispersions split by the Zeeman effect under the magnetic field.

If incident direction is fixed to  $k > 0$ , both dispersion relations in Figs. 1(a) and 1(b) look indistinguishable. Therefore, refraction phenomena in the chiral media can be an optical analog of the atomic beam SG effects in the sense that a beam refracts and splits into two beams with different polarizations. Refraction with a normal incidence requires a nonuniform medium. Suppose a nonuniform medium with the refractive index gradient  $n(x)$  in a direction perpendicular to the incident ( $+z$ ) direction as shown in Fig. 1(c). The variables  $t$  and  $w$  correspond, respectively, to thickness and width of the medium. In the medium, white color represents a smaller refractive index region, whereas dark blue color represents a larger refractive index region. The amount of refraction angle

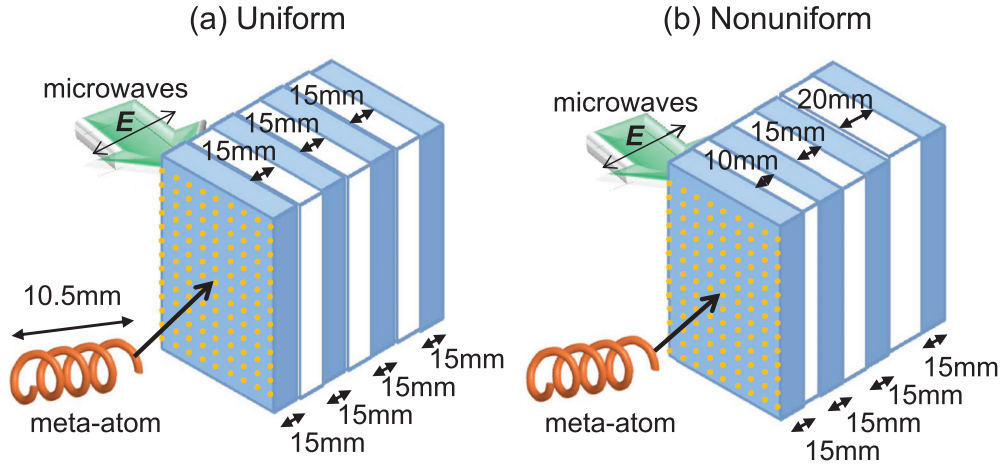


FIG. 2. Schematics of (a) uniform and (b) nonuniform chiral metamaterials consisting of chiral meta-atoms.

$\theta$  through the medium is calculated to be

$$\theta \simeq \Delta n \frac{t}{w}, \quad (10)$$

where  $\Delta n$  is total variation of the refractive index in the  $x$  direction. In a chiral medium, the refractive index depends on the circular polarization states. The split angle of each polarized beam on the first order of  $\xi$  is obtained to be

$$\theta_R - \theta_L = 2\Delta\xi \frac{t}{w}, \quad (11)$$

where  $\Delta\xi$  is variation of the chiral parameter.

As represented in Eqs. (6) and (7), the refractive indices have two terms:  $n_0$  and  $\xi\hat{k}$ . In the present experiment, we embody the spatial variation of these terms in metamaterials. The spatial variation refracts the beam, but the two terms affect the beam in a different way. The gradient in the first term bends the center of gravity of the beam and gives effectively nonzero incident angle. The spatial derivative of the second term causes a split of the beam depending on polarization states, corresponding to the optical analog of the SG effects.

### III. EXPERIMENTAL PROCEDURES

A 0.55 mm diameter Cu wire was coiled clockwise four times round the thread groove of a right-handed screw to form the Cu right-handed chiral meta-atom. The weight of all chiral meta-atoms is identically 76 mg. The length of the meta-atoms was 10.5 mm, which is much smaller than the frequency of microwave we use in the measurements. As illustrated in Fig. 2, the meta-atoms in a  $9 \times 13$  square lattice array were juxtaposed in a polystyrene foam plate of 200 mm  $\times$  200 mm  $\times$  15 mm. The meta-atom's chiral axis is normal to the plate surface. The spacing between the meta-atoms was 15 mm. A polystyrene foam plate contains 117 chiral meta-atoms to be a chiral metalayer. Four chiral metalayers were stacked to construct chiral metamaterials. In order to construct uniform chiral metamaterials, other polystyrene foam plates having 15 mm thickness were inserted between the metalayers as spacers [Fig. 2(a)]. Contrastingly, nonuniform chiral metamaterials were embodied with a gradual increase in the polystyrene foam spacers' thicknesses [Fig. 2(b)]; in other words, 10, 15, and 20 mm thickness polystyrene foam plates were inserted in

a nonuniform chiral metamaterial to mimic the SG-like fields for microwaves.

The chiral metamaterials were put onto a rotation stage. A rectangle horn antenna for microwave emission (Keycom RH187S) was also mounted on the rotation stage. The transmitted microwaves are linearly polarized. As illustrated in Fig. 2, the chiral axis is along the incident electric field oscillation direction in the present free-space experiment, so that the ac electric fields excite a resonance in the chiral meta-atom, called chiral resonance, due to electromagnetic induction. The metamaterials were irradiated by microwaves with the normal incidence as shown in Fig. 2, i.e., the microwave incident angle to the metamaterials was always  $0^\circ$ . The transmitted microwaves through the metamaterials were received by another rectangle horn antenna (ETS-Lindgren 3115) for linearly polarized microwaves or antennas for LHCP/RHCP microwaves at the fixed position about 2.5 m away from the metamaterials. Scattering far-field patterns were measured while the emission antenna mounted on the stage together with the metamaterial was rotated from 0 to  $180^\circ$ . The angle of  $90^\circ$  corresponds to the transmitter antenna to be straight to the receiver antenna. The microwave source and detector in the frequency range between 4.7 and 6 GHz was an Agilent PNA N5224A vector network analyzer.

### IV. EXPERIMENTAL RESULTS

#### A. Uniform chiral metamaterials

Figure 3 shows transmission amplitude spectra between 4.7 and 6 GHz through uniform chiral metamaterials at a rotation stage angle of  $90^\circ$ . In Fig. 3(a) microwaves are received by a rectangle horn antenna. The red spectrum corresponds to the co-polarization configuration, in which the polarization plane of an electric field in the transmitter rectangle horn antenna is parallel to that in the receiver rectangle horn antennas. This configuration results in almost perfect transmission without any samples between antennas. However, Fig. 3(a) obtained with the chiral metamaterials highlights that transmission is suppressed between 4.9 and 5.5 GHz. In the suppressed region, a dip emerged at approximately 5.2 GHz. This dip is traced back to the chiral resonance [18,19,26]. The transmission

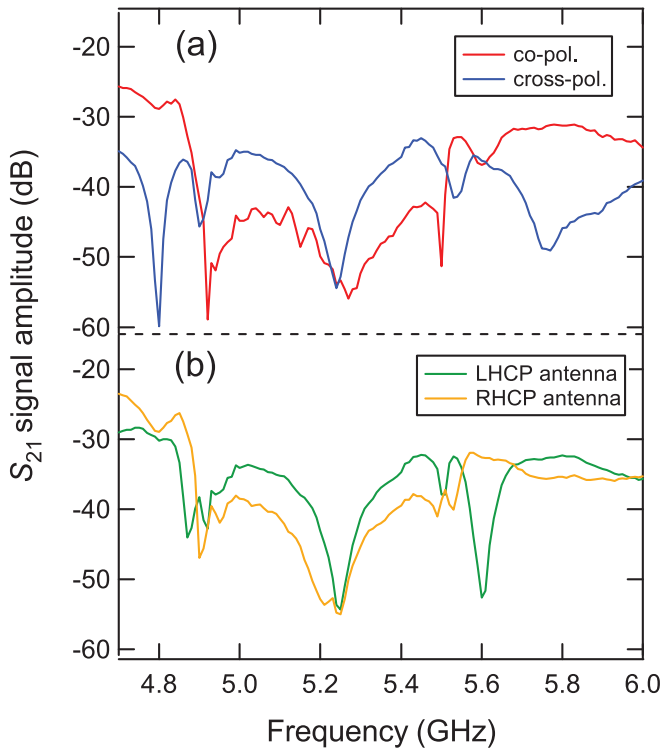


FIG. 3. Transmission amplitude spectra of uniform chiral materials between 4.7 and 6 GHz at  $90^\circ$ . (a) Red and blue spectra correspond to microwaves received by a rectangle horn antenna in co- and cross-polarization configurations, respectively. (b) Green and yellow spectra correspond to microwaves received by LHCP and RHCP antennas, respectively.

suppression between 4.9 and 5.5 GHz is thus caused by the rotation of the microwave polarization plane through the transmission, i.e., optical activities.

The blue spectrum in Fig. 3(a) corresponds to the cross-polarization configuration. In the cross-polarization configuration, the polarization plane of an electric field in the transmitter is normal to that in the receiver antennas. The cross-polarization configuration corresponds to cross Nicol configuration in optics. Hence, if there is nothing between the antennas, no transmission is observed. This configuration, however, enables us to observe the optical activity of the chiral metamaterials. Indeed in Fig. 3(a) transmission amplitude between 4.9 and 5.5 GHz in the cross-polarization (blue) is larger than that in the co-polarization (red) because of the rotation of the polarization plane due to the optical activities by the chiral metamaterials. A dip is seen at approximately 5.2 GHz also in the blue spectrum.

Figure 3(b) illustrates microwave transmission amplitude spectra received by circularly polarized antenna. The green and yellow spectra correspond to the spectra received by LHCP and RHCP antennas, respectively. The LHCP antenna (green) received large transmission between 4.9 and 5.5 GHz rather than the RHCP antenna (yellow). This result sounds contradictory since the chiral meta-atoms in the metamaterials are right-handed. However, this is reasonable because a LHCP antenna means that the direction of time-variant electric field is left-handed, bringing about a right-handed space-variant

electric field. Additionally green and yellow spectra highlight a dip approximately 5.2 GHz. These results indicate that the chiral metamaterials have a resonance at approximately 5.2 GHz and demonstrate the optical activity around the resonance frequency.

Figure 4 demonstrates the scattering far-field patterns of microwaves received by a rectangle horn antenna after uniform chiral metamaterials. Vertical and horizontal axes are assigned to frequency and stage rotation angle, respectively. Vertical broken lines indicate a stage rotation angle of  $90^\circ$  corresponding to microwave scattering received by the antenna to be straight to the transmitter antenna. Figure 4(a) corresponds to a far-field pattern in the co-polarization configuration. Below 4.9 GHz and above 5.5 GHz transmission is observed around  $90^\circ$ . Transmission between 4.9 and 5.5 GHz is suppressed owing to the optical activity of the chiral metamaterials as shown in Fig. 3. Contrastingly, as demonstrated in Fig. 4(b), the cross-polarization configuration results in a microwave transmission between 4.9 and 5.5 GHz around  $90^\circ$  due to the optical activity except for the resonance frequency at approximately 5.2 GHz.

The far-field patterns shown in Fig. 5 were measured by a LHCP/RHCP antenna after uniform chiral metamaterials. Figure 5(a) corresponds to a far-field pattern received by the LHCP antenna. Around  $90^\circ$ , microwave transmission is observed between 4.7 and 6.0 GHz except for the resonance frequency at approximately 5.2 GHz. Given that the LHCP antenna receives space-variant RHCP microwaves, the transmission is observed in the optical activity region between 4.9 and 5.5 GHz in Fig. 5(a). In sharp contrast in Fig. 5(b), the RHCP antenna cannot receive microwaves in the optical activity region. Notably, the far-field patterns in Fig. 4 and Fig. 5 are symmetrical with the stage rotation angle of  $90^\circ$  because the refractive index in the chiral metamaterials is uniform. However, the far-field patterns become asymmetric when the microwaves scattered by nonuniform chiral metamaterials with a refractive index gradient as shown in the following.

## B. Nonuniform chiral metamaterials

Figure 6 illustrates microwave scattering far-field patterns through nonuniform chiral metamaterials measured by the circularly polarized antennas. Transmission amplitude is plotted as a function of the rotation stage angle (horizontal axis) and frequency (vertical axis). Figures 6(a) and 6(b) correspond to the far-field patterns of a nonuniform chiral metamaterial with spacers of 10, 15, and 20 mm thickness from the  $180^\circ$  side; in other words, a graded chiral metamaterial with a higher density of the chiral meta-atoms in the  $180^\circ$  direction. Out of the optical activity region between 4.9 and 5.5 GHz, far-field patterns received with the LHCP [Fig. 6(a)] and RHCP [Fig. 6(b)] antennas are similar. Below the optical activity region, the microwaves transmit and deflect in the  $180^\circ$  direction. On the other hand, the transmitted beam shifts in the  $0^\circ$  direction above the optical activity region. These deflections are caused by the refractive index gradient perpendicular to the microwave propagation in the metamaterials. Above the chiral resonance frequency at approximately 5.2 GHz, the electric permittivity of the metamaterials becomes negative and the beam deflects in the opposite direction to the

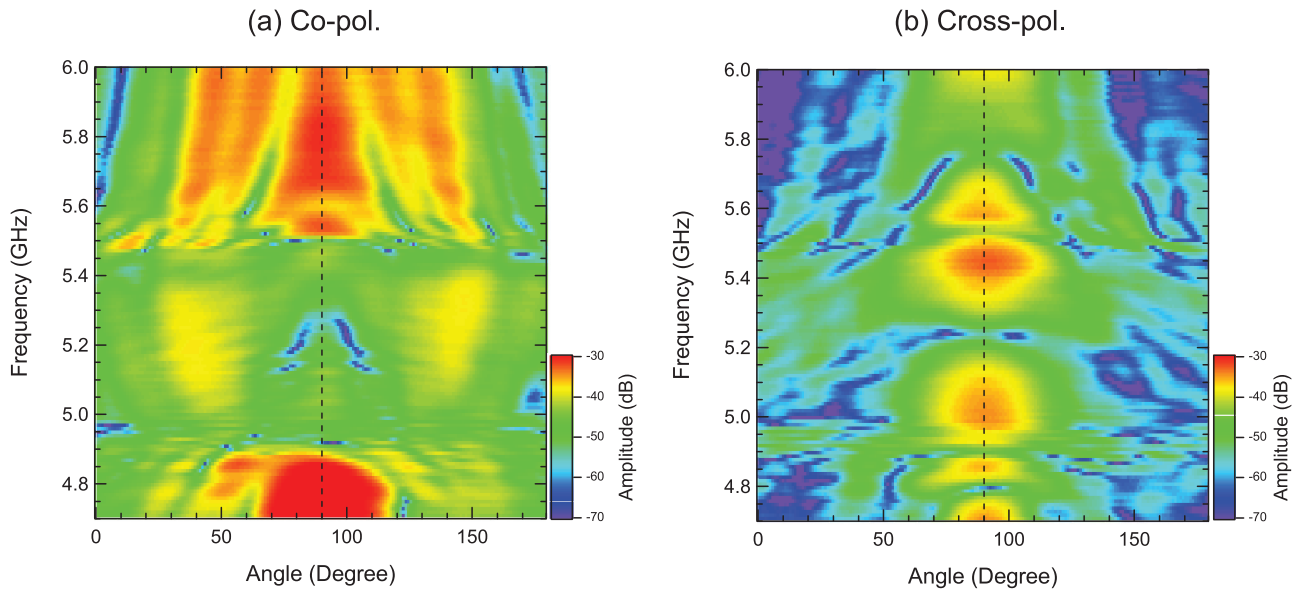


FIG. 4. Microwave scattering far-field patterns of uniform chiral metamaterials. Transmission amplitude is plotted as a function of rotation angle (horizontal axis) and frequency (vertical axis). Vertical broken lines indicate  $90^\circ$ . Microwaves are received by rectangle horn antenna in (a) co- and (b) cross-polarization configurations.

metamaterials with positive permittivity below the chiral resonance frequency.

In the optical activity region, the far-field patterns are very different between the LHCP [Fig. 6(a)] and RHCP [Fig. 6(b)] antennas. Figure 6(a) demonstrates the high transmission of microwaves in the optical activity region between 4.9 and 5.5 GHz. In contrast, the RHCP antenna does not receive large transmission as shown in Fig. 6(b). The far-field pattern in the optical activity region is asymmetric due to the refractive index gradient in the chiral metamaterials. Just below the chiral resonance frequency of approximately 5.2 GHz, the LHCP antenna detects microwaves around  $140^\circ$  because of a higher

density of the chiral meta-atoms in the  $180^\circ$  direction. On the other hand at approximately 5.3 GHz just above the chiral resonance frequency, microwaves are detected at around  $50^\circ$ . While the density of the meta-atoms is higher in the  $180^\circ$  direction, the permittivity becomes negative above the chiral resonance, leading to a deflection into the  $0^\circ$  direction.

Figures 6(c) and 6(d) correspond to far-field patterns through inverted nonuniform chiral metamaterials with 10, 15, and 20 mm thick spacers from  $0^\circ$ ; in other words, a graded chiral metamaterial with a higher chiral meta-atom density in the  $0^\circ$  direction. The flip of the refractive index gradient direction brings about mirror images of the transmission

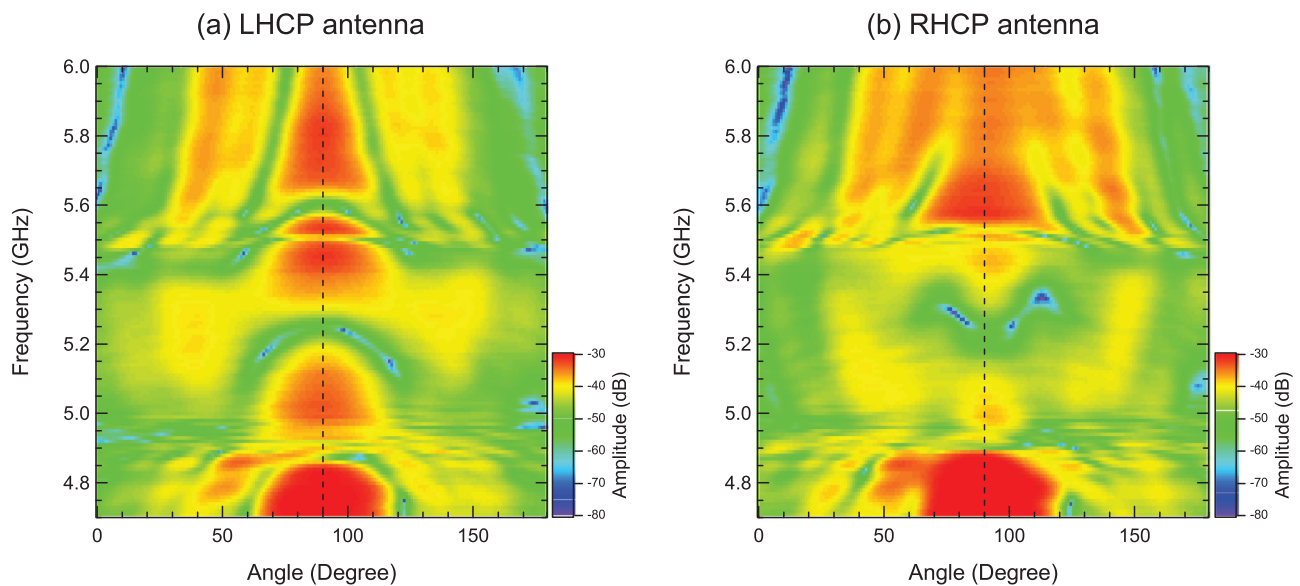


FIG. 5. Microwave scattering far-field patterns of uniform chiral metamaterials received using (a) LHCP and (b) RHCP antennas. Transmission amplitude is plotted as a function of rotation angle (horizontal axis) and frequency (vertical axis). Vertical broken lines indicate  $90^\circ$ .

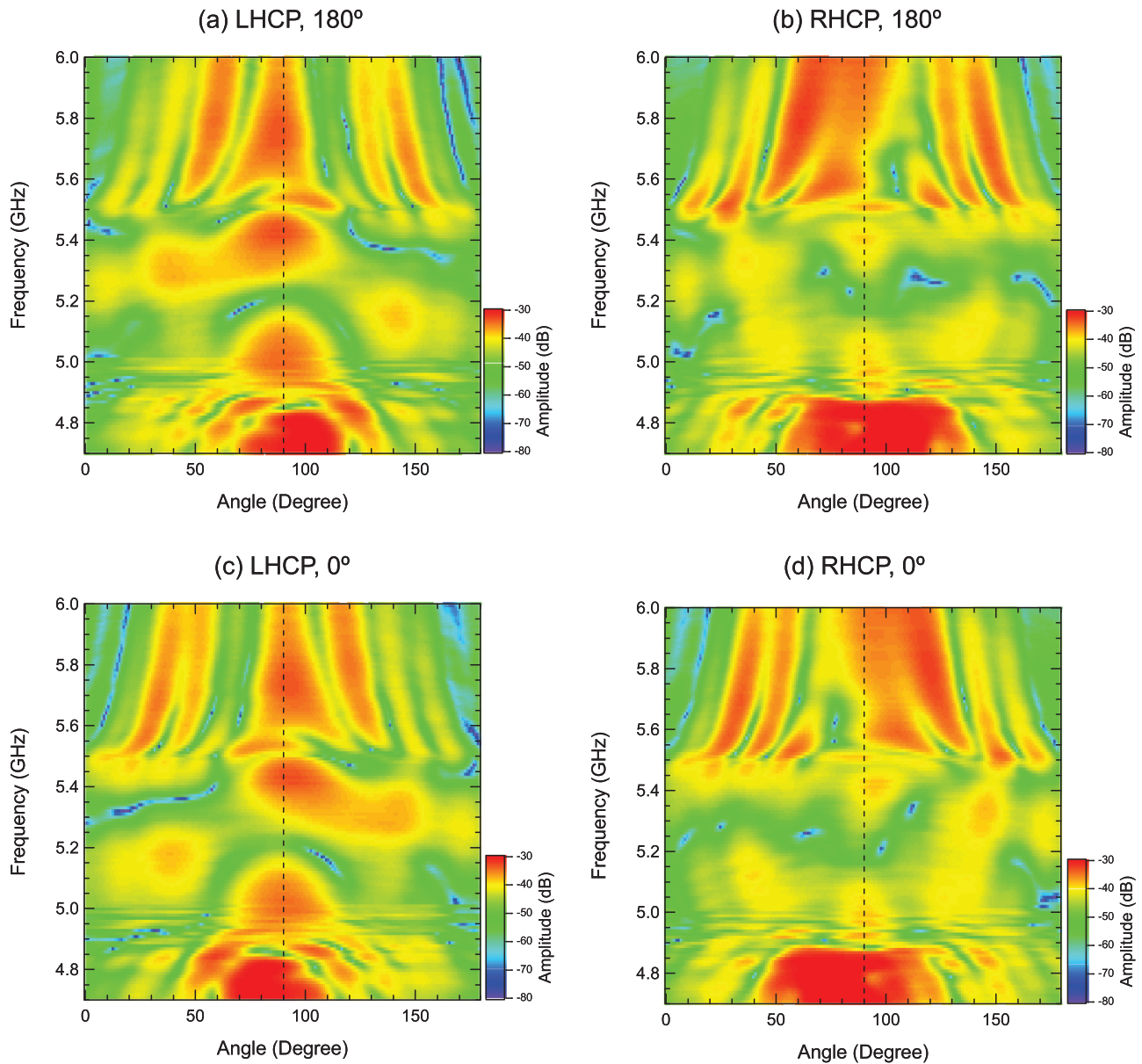


FIG. 6. Microwave scattering far-field patterns of nonuniform chiral metamaterials received using LHCP [(a) and (c)] and RHCP [(b) and (d)] antennas. (a), (b) Density of chiral meta-atom is higher in  $180^\circ$ . (c), (d) Density of chiral meta-atom is higher in  $0^\circ$ .

patterns by comparing Figs. 6(a) and 6(c) and Figs. 6(b) and 6(d). In the optical activity region between 4.9 and 5.5 GHz, microwave transmission is high around  $50^\circ$  just below the chiral resonance frequency, whereas the transmission is high around  $140^\circ$  just above the chiral resonance frequency. These results demonstrate that microwaves feel the refractive index gradient in the nonuniform chiral metamaterials and are deflected in to the direction of a higher refractive index due to a higher meta-atom density.

## V. DISCUSSION

Figure 7 shows the amplitude difference between transmitted microwaves received by LHCP and RHCP antennas after the uniform chiral metamaterial. The pattern is plotted as a function of stage rotation angle (horizontal axis) and

frequency (vertical axis). The vertical broken line indicates the rotation angle of  $90^\circ$ , while the horizontal broken line indicates 5.2 GHz, which corresponds to the chiral resonance of the meta-atoms. Red color is assigned to amplitude difference above 15 dB corresponding to a higher transmission detected by the LHCP antenna. On the other hand, blue color is assigned to amplitude difference below  $-15$  dB corresponding to a higher transmission detected by the RHCP antenna. We see that the LHCP antenna received intense microwaves at a frequency just below 5.2 GHz around the rotation angle of  $90^\circ$ . This result is consistent with the spectra measured in Fig. 3(a). Notably in Fig. 7 the amplitude difference pattern is symmetric by the uniform chiral metamaterials. Contrastingly, nonuniform chiral metamaterials cause asymmetric patterns in amplitude difference as highlighted in Fig. 8.

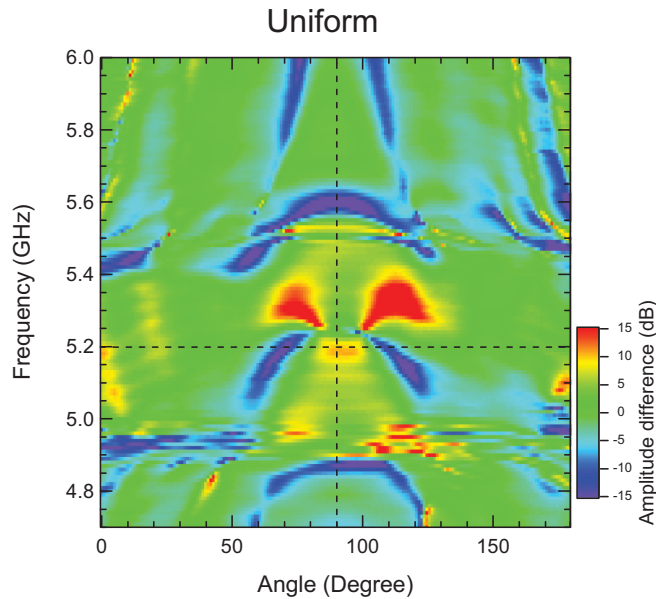


FIG. 7. Amplitude difference between transmitted microwaves measured by LHCP and RHCP antennas after uniform chiral metamaterial is plotted as a function of stage rotation angle (horizontal axis) and frequency (vertical axis). Red color corresponds to high transmission detected by LHCP antenna, while blue color corresponds to high transmission detected by RHCP antenna. Vertical broken line indicates  $90^\circ$ . Horizontal broken line indicates chiral resonance frequency of 5.2 GHz.

Figure 8 plots a similar amplitude difference transmission pattern but through the nonuniform chiral metamaterial. Figure 8(a) corresponds to metamaterials with a high density of meta-atoms in the  $0^\circ$  direction. The most striking asymmetric pattern is observed at approximately 5.35 GHz in the optical activity region. Strong transmission around  $120^\circ$  is measured with the LHCP antenna. On the other hand, the RHCP antenna detects transmission around  $60^\circ$  at the same frequency.

By reversing the gradient direction, the asymmetric pattern is flipped as shown in Fig. 8(b). At approximately 5.35 GHz, strong transmission around  $70^\circ$  is measured by the LHCP antenna while transmission around  $120^\circ$  is detected by the RHCP antenna. Figure 8 demonstrates that circularly polarized light with opposite “spins” go their separate ways in the nonuniform chiral metamaterials. In other words, we have observed directly the SG effects for microwaves by nonuniform chiral metamaterials.

The original SG experiment using an atomic beam [1] showed that particles with opposite electron spins with nonzero magnetic moments went their separate ways in a magnetic field gradient perpendicular to the atomic beam. In the optical analog demonstrated in this paper, LHCP and RHCP microwaves are deflected by the refractive index gradient perpendicular to the microwave propagation realized by nonuniform chiral metamaterials. As represented in Eqs. (6) and (7), LHCP and RHCP microwaves feel different values of  $\xi$ , resulting in propagations in their separate ways. The splitting is traced back to “magnetic field” for microwaves because the gauge field and nonuniform magnetic field in the original SG experiment correspond to electromagnetic induction by chiral materials

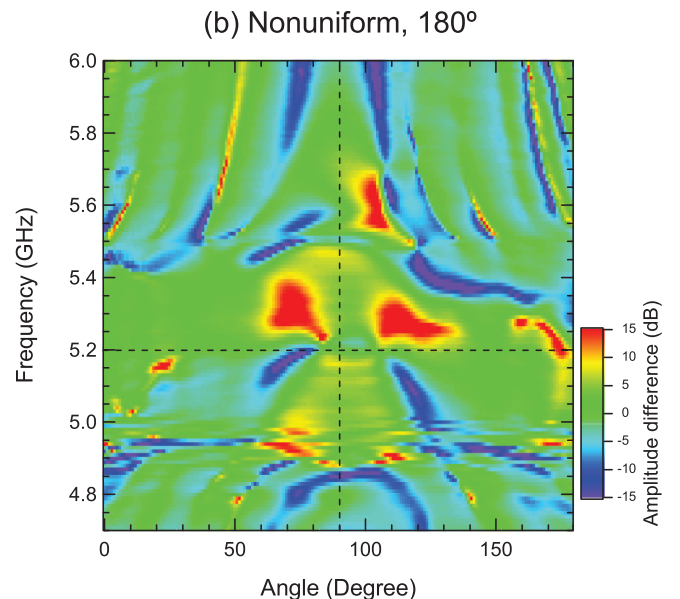
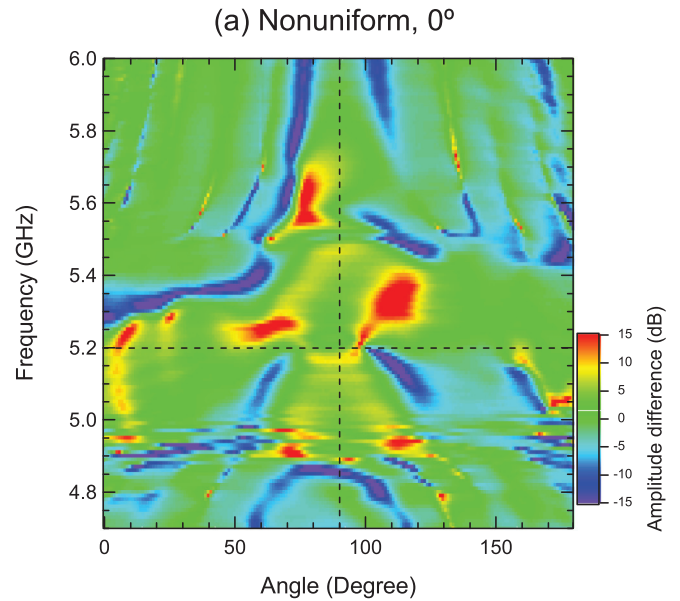


FIG. 8. Amplitude difference pattern measured by LHCP and RHCP antennas after nonuniform chiral metamaterial is plotted as a function of angle (horizontal axis) and frequency (vertical axis). Meta-atoms concentrations are dense in the  $0^\circ$  (a) and  $180^\circ$  (b).

and the nonuniform distribution of the chiral meta-atoms in the present experiment, respectively. In this way, the present experiment is an evidence of synthetic magnetic field for light [20–25] at room temperature using metamaterials.

Notably, a similar behavior of microwaves can be realized using graded anisotropic materials. However, in anisotropic materials, circular polarizations are not eigenstates. We utilized chiral metamaterials to make a direct analogy between circular polarizations (LHCP and RHCP) of microwaves and spins (up and down) of electrons. Additionally, our optical analog of Stern-Gerlach effects by nonuniform metamaterials is applicable to other metamaterials, for example, magneto-optical metamaterials [27]. Last but not least, we notice that

an optical SG effect has been reported [28]. In the optical SG effect, a metastable He atoms beam interacts with a resonant laser field with a well-defined intensity gradient perpendicular to the atomic beam. The optical SG effect is thus completely different from what we observed in the present study.

## VI. CONCLUSION

In conclusion, a microwave analog of the SG effects was realized using nonuniform chiral metamaterials. Nonuniform chiral metamaterials with a refractive index gradient were constructed using the chiral meta-atoms that exhibit optical activities at microwave frequencies. Microwave scattering

far-field patterns with a normal incidence into nonuniform chiral metamaterials highlight a deflection of transmitted microwaves. Moreover, circularly polarized microwaves with opposite “spins of light” go their separate ways in the nonuniform chiral metamaterial. The splitting is traced back to magnetic field for microwaves. The present study thus opens a way for synthetic gauge fields for light using metamaterials.

## ACKNOWLEDGMENTS

The authors acknowledge financial support of this work by JSPS KAKENHI (Grants No. 26287065 and No. 16K04881) and a grant from the Research Foundation for Opto-Science and Technology.

- 
- [1] W. Gerlach and O. Stern, *Z. Phys.* **8**, 110 (1922).
  - [2] J. J. Sakurai and J. J. Napolitano, *Modern Quantum Mechanics* (Pearson Education Limited, Harlow, 2013).
  - [3] L. Karpa and M. Weitz, *Nat. Phys.* **2**, 332 (2006).
  - [4] D. L. Zhou, L. Zhou, R. Q. Wang, S. Yi, and C. P. Sun, *Phys. Rev. A* **76**, 055801 (2007).
  - [5] L. Zhou, J. Lu, D. L. Zhou, and C. P. Sun, *Phys. Rev. A* **77**, 023816 (2008).
  - [6] Y. Guo, L. Zhou, L.-M. Kuang, and C. P. Sun, *Phys. Rev. A* **78**, 013833 (2008).
  - [7] A. J. Fresnel, in *Œuvres complètes d’Augustin Fresnel*, edited by H. d. Sénarmont, E. Verdet, and L. Fresnel (Imprimerie impériale, Paris, 1866), Vol. 1.
  - [8] E. Hecht, *Optics* (Pearson Education Limited, Harlow, 2013).
  - [9] J. A. Kong, *Electromagnetic Wave Theory* (EMW Publishing, Cambridge, 2005).
  - [10] R. W. Ditchburn, *Light* (Dover Publications, New York, 1991).
  - [11] A. Ghosh and P. Fischer, *Phys. Rev. Lett.* **97**, 173002 (2006).
  - [12] D. R. Smith, J. B. Pendry, and M. C. K. Wiltshire, *Science* **305**, 788 (2004).
  - [13] D. Schurig, J. J. Mock, B. J. Justice, S. A. Cummer, J. B. Pendry, A. F. Starr, and D. R. Smith, *Science* **314**, 977 (2006).
  - [14] N. I. Landy, S. Sajuyigbe, J. J. Mock, D. R. Smith, and W. J. Padilla, *Phys. Rev. Lett.* **100**, 207402 (2008).
  - [15] N. Yu, P. Genevet, M. A. Kats, F. Aieta, J.-P. Tetienne, F. Capasso, and Z. Gaburro, *Science* **334**, 333 (2011).
  - [16] M. Kang, T. Feng, H.-T. Wang, and J. Li, *Opt. Express* **20**, 15882 (2012).
  - [17] S. Xiao, J. Wang, F. Liu, S. Zhang, X. Yin, and J. Li, *Nanophotonics* **6**, 215 (2016).
  - [18] S. Tomita, K. Sawada, A. Porokhnyuk, and T. Ueda, *Phys. Rev. Lett.* **113**, 235501 (2014).
  - [19] S. Tomita, H. Kurosawa, K. Sawada, and T. Ueda, *Phys. Rev. B* **95**, 085402 (2017).
  - [20] K. Sawada and N. Nagaosa, *Phys. Rev. Lett.* **95**, 237402 (2005).
  - [21] M. Hafezi, E. A. Demler, M. D. Lukin, and J. M. Taylor, *Nat. Phys.* **7**, 907 (2011).
  - [22] K. Fang, Z. Yu, and S. Fan, *Nat. Photon.* **6**, 782 (2012).
  - [23] A. B. Khanikaev, S. H. Mousavi, W.-K. Tse, M. Kargarian, A. H. MacDonald, and G. Shvets, *Nat. Mater.* **12**, 233 (2013).
  - [24] L. Lu, L. Fu, J. D. Joannopoulos, and M. Soljačić, *Nat. Photon.* **7**, 294 (2013).
  - [25] M. Hafezi, S. Mittal, J. Fan, A. Migdall, and J. M. Taylor, *Nat. Photon.* **7**, 1001 (2013).
  - [26] K. F. Lindman, *Ann. Phys.* **368**, 621 (1920).
  - [27] M. Sadatgol, M. Rahman, E. Forati, M. Levy, and D. Ö. Güney, *J. Appl. Phys.* **119**, 103105 (2016).
  - [28] T. Sleator, T. Pfau, V. Balykin, O. Carnal, and J. Mlynek, *Phys. Rev. Lett.* **68**, 1996 (1992).